

# Modeling of Ballistic Impact of Fragment Simulating Projectiles against Aluminum Plates

Teresa Fras, Leon Colard, Bernhard Reck

French-German Research Institute of Saint-Louis (ISL),  
5 rue du General Cassagnou, 68301 Saint-Louis,  
France

## 1 Abstract

In this paper, the ballistic impact test is described in which fragment simulating projectiles (FSPs) have been used against thick plates made of an aluminum alloy. To perforate the plates, the projectiles must have reached velocities higher than 890m/s. The failures of targets are modeled in the numerical simulation using the Lagrangian Finite Elements Method with the Johnson – Cook constitutive model coupled with the cumulative-damage fracture model implemented in the \*MAT\_107.

**\*KEYWORDS: BALLISTIC IMPACT TEST, ALUMINUM, FRAGMENT SIMULATING PROJECTILE (FSP), LAGRANGIAN SOLVER, \*MAT\_107**

## 2 Introduction

Light metal alloys offer a good resistance to impacts together with a relatively low density, which fulfills a basic condition for optimized ballistic shields. The good mechanical and physical properties, low density and corrosion resistance make aluminum alloys the important components of many light weight protective structures. In general, the Al alloys of 7xx series are characterized by a lack of corrosion and a good strength - weight ratio. Due to such mechanical and physical properties, the alloys can be subjected to extreme environmental exposures, including both low and high temperatures, high pressures and highly corrosive and reactive fluids, [1]. Consequently, one member of this alloy family, the AA7020-T651, is widely used in welded structural components, in military and aerospace applications.

To verify the ballistic performance of the discussed alloy, the impact test with Fragment Simulating Projectiles (FSPs) were performed and analyzed. Fragment Simulating Projectiles are standard military penetrators of a non-axisymmetric geometry used to simulate artillery shell fragments, [2]. Dimensions and material properties of this kind of projectiles fulfill the requirements of Military Specification MIL-P-46593A, [3]. 20 mm FSPs simulate 155mm artillery shell fragments in procedures of evaluating the protection level of logistic and light armored vehicles described in [4]. Deformation caused by a normal impact of FSP is analyzed in reports addresses mainly for military purposes. Consequently, such investigations are less frequent than articles discussing deformation caused by blunt-, round- or ogive- nose projectiles. The analysis of a target deformation caused by a FSP projectile is a complementary study to the already existing reports concerning target response to impacts of the projectiles of other shapes.

In order to understand the mechanisms occurring in a material subjected to the impact, it is necessary to know its mechanical properties and conditions leading to its failure. The throughout material investigation has been performed for AA7020-T651, on the basis of which, a thermoviscoplastic constitutive model and a fracture criterion are determined by using the Johnson-Cook model, [5], and the corresponding fracture criterion, [6]. This material model is implemented in the Lagrangian Finite Element Method provided by LS-DYNA (via \*MAT\_107\_MODIFIED\_JOHNSON\_COOK), [7]. The numerical simulation of the ballistic impact test aims to analyze the material behavior under high velocity impact. The obtained observations and conclusions, confirmed by the numerical modeling, may be useful for an evaluation and development of lightweight and cost-effective protection systems.

### 3 Experimental investigation

The experimental investigation is realized by means of 40 mm thick plates impacted by the 20 mm - diameter Fragment Simulating Projectiles (FSPs), Fig. 1(b). The target specimens were delivered as cylindrical samples of 40 mm thickness. They were pressed inside an aluminum frame (made of the commercial alloy AA6061-T651) due to which samples are stabilized for shots, [8] Fig. 1(a). Such a configuration allows samples of reduced size to be tested. Specimens are considered as thick because a ratio of their thickness compared to an impactor diameter is equal to 2, i.e.  $H_{\text{plate}} / R_{\text{projectile}} = 2$  [9].

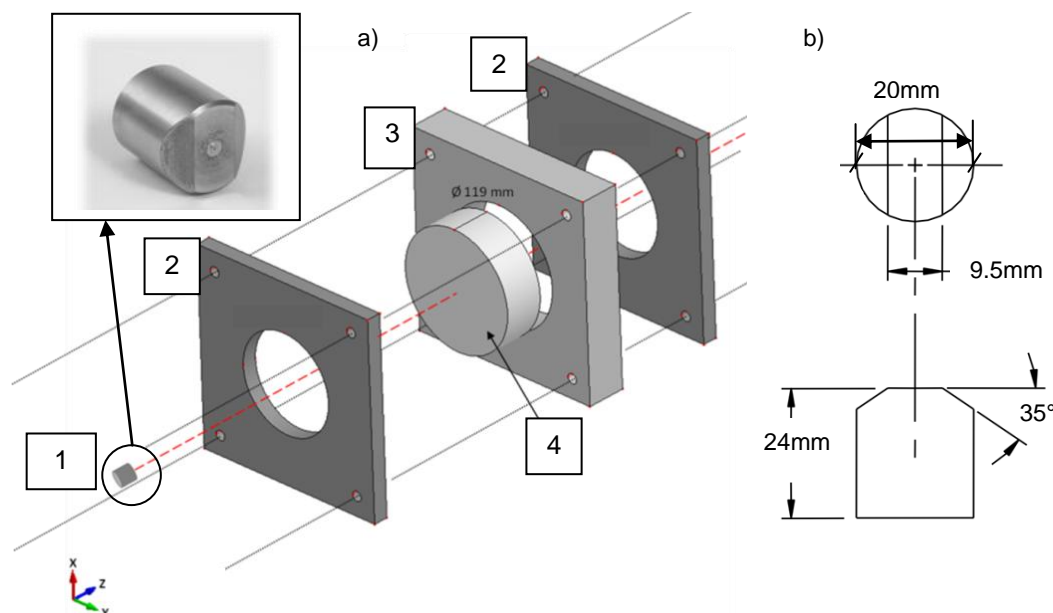


Fig. 1: (a) Experimental configuration for impact tests: 1) projectile, 2) steel frames, 3) aluminum frame, 4) target. (b) Geometry of FSP.

The ballistic limit for the given target/projectile configuration is determined from the relation between the initial ( $v_0$ ) and residual ( $v_R$ ) projectile velocities, Fig. 2(a). The ballistic limit velocity, i.e. the greatest impact velocity the target can withstand without being perforated, is close to  $v_{\text{bl.exp}} \approx 890$  m/s. The experimental data are fitted to a model proposed by Lambert (1978) [9]. With increasing impact velocity, the observed failure modes of the target plates change from plugging ( $v_{\text{impact}} < 1200$  m/s) to discing ( $v_{\text{impact}} > 1200$  m/s). A plug is a part of a metallic material which is sheared out from a target plate by a deformed projectile, Fig. 2(c). Discing leads to a material separation within same planes, parts of such planes are thrown away from a target, Fig. 2(b). Such failure modes are characteristic for a ductile, anisotropic material, when the texture influences a fracture direction, [10].

During the penetration, the global deformation mode of a target changes from a ductile hole enlargement, through a mechanism of highly localized shear around the projectile nose, to a combination of plugging and discing (scabbing) mode. In the initial stage of the deformation, the target material is pushed to the sides and compressed in front of the projectile - causing an enlargement of the penetration channel. The target material moves ahead of the projectile leading to the bulge formation on the rear plate surface. The large shear strains develop in the target at the periphery of the projectile, highly localized shear bands occur and the process changes to a plug formation, which final step is a plug ejection. Impact velocities higher than 1200 m/s lead to greater plate deformations and to a discing (scabbing) failure mechanism. According to [10], this kind of fracture is caused by a shear mechanism as this fracture takes place along planes which appear to be bands of intense shear and which are also intersected by another set of intense shears. A remained plate thickness, below the projectile, is stretched and bended forward. Bending takes place more easily because it is presented over a series of thin layers (resulting from the subsequent processes of rolling during the material manufacturing) remaining at the rear side of a target plate.

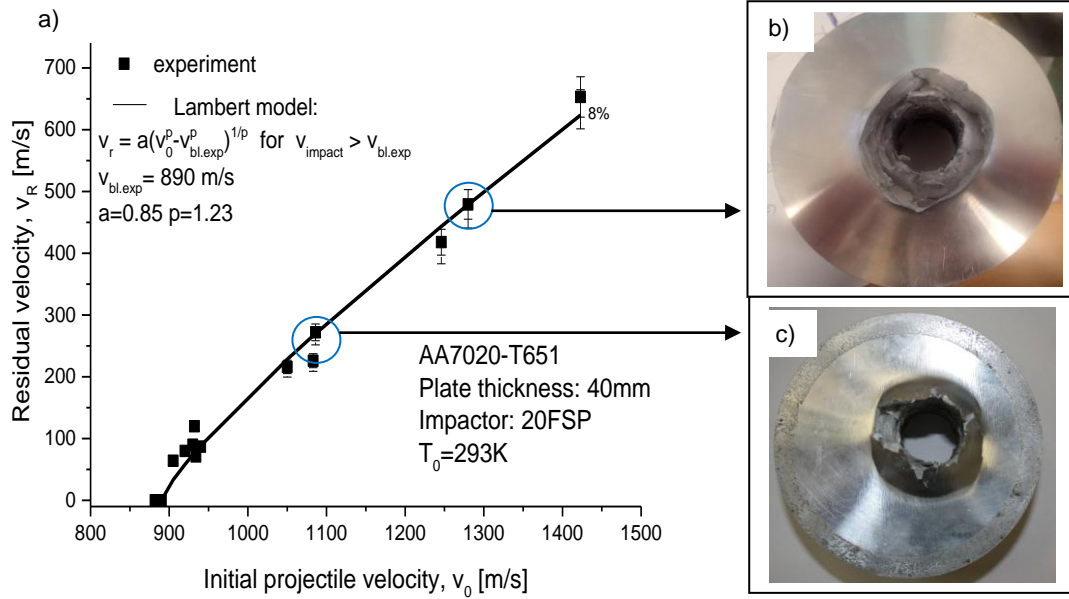


Fig.2: (a) Ballistic curve for 40 mm thick plates of AA7020-T651 impacted by 20 mm FSPs at ambient temperature. Plates deformed due to impacts of FSPs with an initial velocity close (b) 1300 m/s and to (c) 1100 m/s.

#### 4 Numerical simulation and its results

The numerical simulation can be considered as a tool which makes the understanding of ballistic phenomena easier, under the condition that a material model and a fracture criterion are based on a proper material characterization. In this study, the Johnson and Cook constitutive model coupled with a fracture criterion [5 - 6], Eqs. (1) - (3), are used to apply the phenomenological models describing a ductile material behavior and the accumulation of damage in a material. The constitutive model, which is formulated within the framework of viscoplasticity and continuum damage mechanics, allows large plastic strains, high strain rates and temperature effects to be accounted for in the calculations. The equivalent stress depending on the strain, strain rate and temperature is defined as:

$$\sigma(\varepsilon, \dot{\varepsilon}, T) = \left[ A + B\varepsilon^n \right] \left[ 1 + C \ln \frac{\dot{\varepsilon}}{\varepsilon_{ref}} \right] \left[ 1 - \left( \frac{T - T_0}{T_m - T_0} \right)^m \right] \quad (1)$$

where A, B, C, m, n are material constants and  $T_0$ ,  $T_m$  – reference and melting temperature.

Johnson and Cook [6] proposed also a function describing the fracture strain depending on the stress triaxiality, strain rate and temperature. The function is given in Eq. (2).

$$\varepsilon_f(\sigma^*, \dot{\varepsilon}, T) = \left[ D_1 + D_2 e^{D_3 \sigma^*} \right] \left[ 1 + D_4 \ln \dot{\varepsilon} \right] \left[ 1 + D_5 \frac{T - T_0}{T_m - T_0} \right] \quad (2)$$

where  $D_1 - D_5$  are fracture model constants,  $\sigma^*$  is the stress triaxiality ratio.

Since the damage evolution is related to irreversible strain, it may be taken as a function of the accumulated plastic strain. Experiments indicate that the damage remains equal to zero during the growth of dislocations, [11 - 12]. The damage starts to evolve at a certain threshold of the accumulated plastic strain. Consequently, the extended Johnson-Cook damage evolution rule is given by Eq. (3).

$$\dot{D} = \begin{cases} 0 & \text{when } \varepsilon < p_d \\ \frac{D_c}{\varepsilon_f - p_d} \dot{\varepsilon} & \text{when } \varepsilon \geq p_d \end{cases} \quad (3)$$

where  $D_c$  is the critical damage,  $p_d$  is the damage threshold and  $\varepsilon_f$  is the fracture strain.

In order to allow a crack growth during a penetration process, the model is coupled with an element - kill algorithm. As the damage variable  $D$  reaches its critical value  $D_c$ , ( $D_c = 1$  in this case) a damaged element is removed from the mesh.

The parameters of the constitutive relation, Eq (1), are determined on the basis of a mechanical and thermal analysis of the properties of the target material AA7020-T651. The values of Eq. (1) were obtained from our own experimental investigation. The parameters  $D_1 - D_3$  of the fracture strain, Eq. (2), are also obtained from our own experimental results. Whereas, the values  $D_4 - D_5$  are chosen from a set of parameters describing the fracture of an alloy AA7075-T651. This alloy is estimated to present a similar behavior as the analyzed alloy, since it belongs to the same series of Al alloys, i.e. 7xxx, [13]. The parameters are collected in Table 1.

AA7020-T651	A (MPa)	B (MPa)	n	C	m	T <sub>m</sub> (K)	Reference strain rate (s <sup>-1</sup> )
	295	260	1.65	0.000889	1.26	880	0.0001
	D <sub>1</sub>	D <sub>2</sub>	D <sub>3</sub>	D <sub>4</sub>	D <sub>5</sub>	D <sub>c</sub>	P <sub>d</sub>
	0.011	0.42	-3.26	0.016	1.1	1.0	0
	ρ [kg/m <sup>3</sup> ]	G [GPa]	E [GPa]	ν [-]	C <sub>p</sub> [J/kg.K]	Hardness	
	2770	25	71	0.3	452	133 HV ± 2.0	

Table 1. The parameters of Eqs. (1) - (2) for AA7020-T651 and its some physical properties.

FPS is made of AISI 4340-H steel alloy. The material constants for the JC material model are taken from the study of Johnson and Cook [5].

The aim of the simulation is to examine the ability of the computational model to predict the target responses obtained experimentally, which are – plugging (resulting from a highly localized shearing) and discing (occurring for a higher impact velocity and resulted from bending and shearing processes). An explicit solver of the non-linear finite element code provided by LS-DYNA is used. The Johnson - Cook constitutive model and fracture criterion, Eqs. (1) – (3), are implemented in the code via \*MAT\_107\_MODIFIED\_JOHNSON\_COOK, [7, 14]. The detailed description of the model and a large number of examples which present satisfying results of a ballistic impact modeling can be found in [11 - 16]. The numerical model describes linear elasticity, a von Mises plasticity and initial yielding, strain hardening, strain-rate hardening, damage evolution and fracture. The constitutive behavior and the fracture process of the material are assumed to be isotropic. The material anisotropy and the material texture of the aluminum plates are assumed to be negligible in the numerical calculations.

The geometrical model is prepared using 3D solid elements, since FSPs have a non-axisymmetric shape. A further advantage of a 3D model over 2D model is an ability to present the macroscopic damage and fracture modes of the target. Due to the symmetries of geometry and load case, only a quarter of the configuration is modeled, Fig. 3. The 8-node constant-stress solid elements with one integration point and stiffness-based hourglass control are applied. The frame is fully clamped, the plate is in contact with the frame (\*AUTOMATIC\_SURFACE\_TO\_SURFACE) and an initial velocity is applied to the projectile. Contact between the target and projectile is modeled using an eroding algorithm (\*ERODING\_SURFACE\_TO\_SURFACE). Friction between parts is not considered. The target mesh is gradually refined to the centre of the plate which is also the center of impact. The target model results in about 300000 elements, the mesh of a projectile contains about 28000 elements,

whereas the supporting frame consists of 2500 elements. To minimize the mesh dependency of the results, the function \*MAT\_NON\_LOCAL is used with the parameter values suggested by User Manual,  $p=8$  and  $q=2$ , [7, 17]. To model the projectile, a fine mesh using linear hexahedral elements of a size  $0.6 \times 0.6 \times 0.6$  mm is applied. The projectile deformation is determined by means of the JC model defined in the code by its simplified version (\*MAT\_98\_SIMPLIFIED\_JOHNSON\_COOK). The elements are eroded when the effective plastic strain at failure reaches an assumed value, in this case  $p_{fail}=1.0$ .

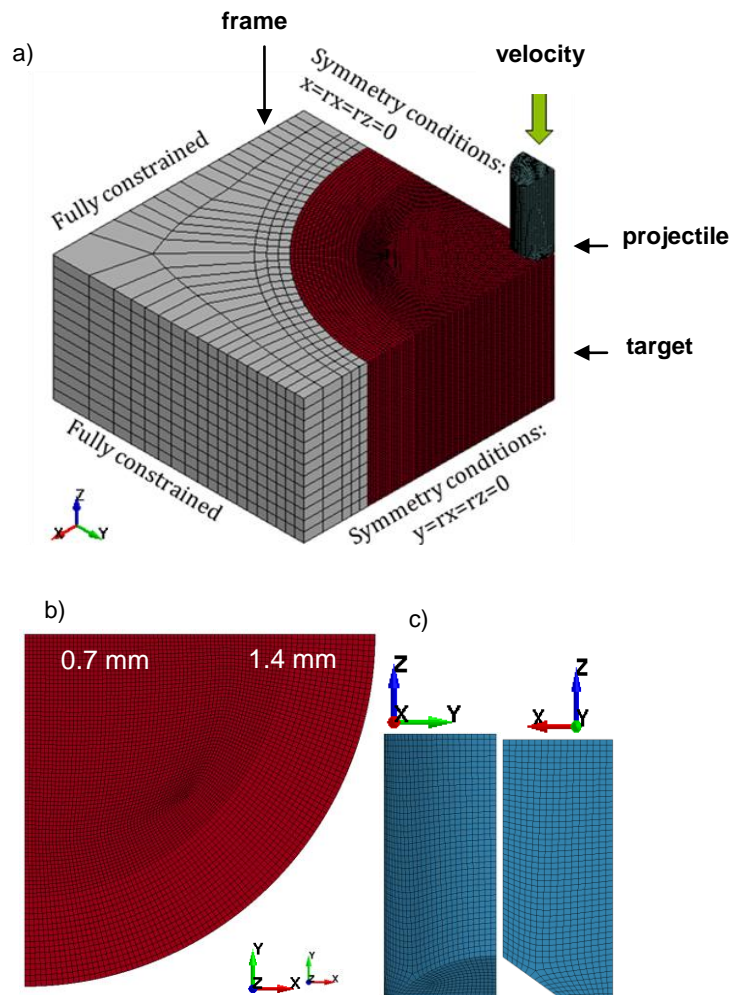


Fig.3: (a) Boundary conditions and mesh details of (a) target plate and (c) projectile..

Deformation resulting from the impact is reproduced by the numerical model. Fig. 4 shows a comparison between the numerical model of a plate which failed due to the impact of a projectile at initial velocity of 1300 m/s and its experimental equivalent. On a front face of the deformed plate, the crater has been created with flanged edge. Parts of materials from the rear face of a plate are torn away – creating a characteristic shape of the discing failure. The cracks occurring regularly inside the penetration channel are not obtained in the numerical simulation but the calculated strains induced by the impact are so large that cracks are initiated.

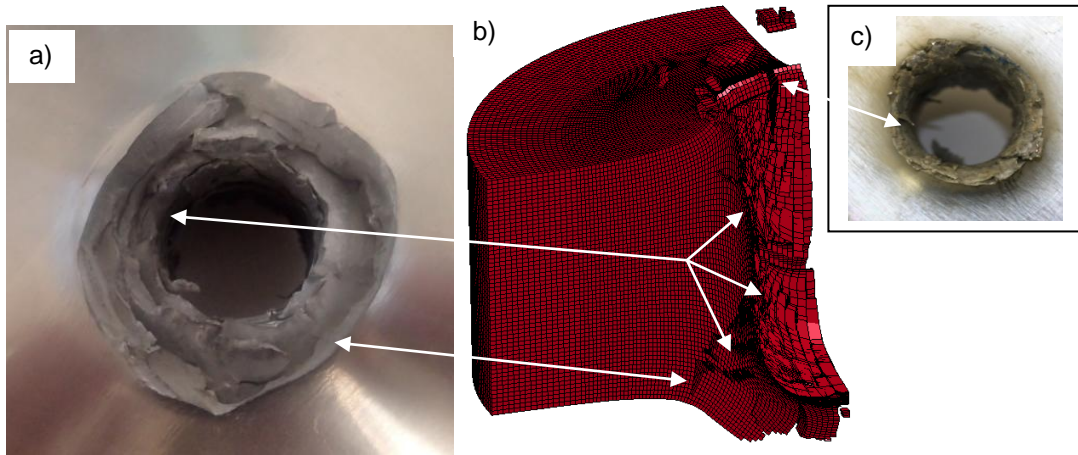


Fig.4: Calculated discing failure mode and its comparison with a plate failed due to an impact with an initial velocity 1300 m/s: a) rear plate face, b) numerical results, c) projectile entry.

In Fig. 5, the maps of increasing values of the damage parameter  $D$  are shown. The figure presents the subsequent plots of the mesh deformation during the penetration caused by a FSP impact leading to a bulge formation, Fig. 5(a) – (b), shear localization, Fig. 5(c) – (d), and to the final perforation of the target plate, Fig. 5(d).

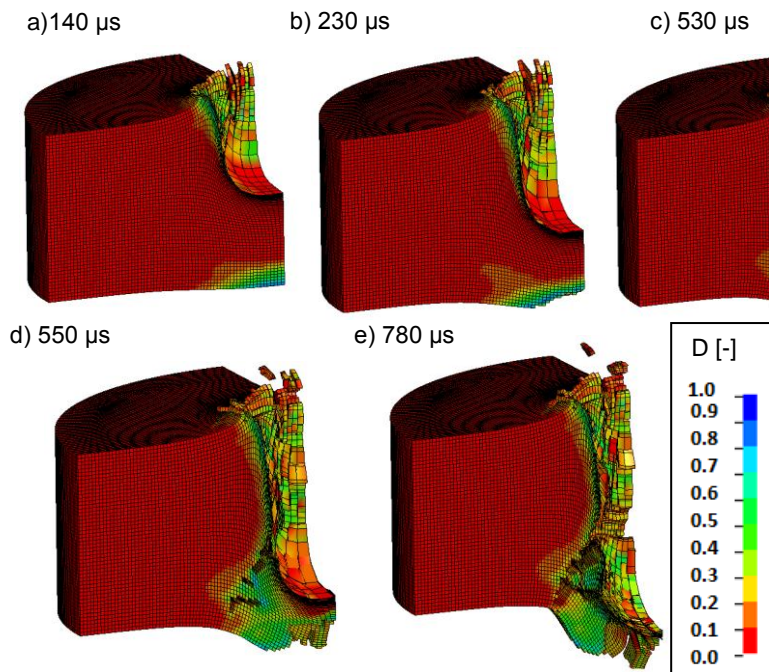


Fig.5: Mesh deformation presented in maps of damage parameter  $D$ .

When the projectile indents the target, the target mass in front of the projectile is accelerated. The momentum of the projectile results in compression of the material in front of the projectile nose and in shearing of the material in the zone surrounded the projectile. The bottom part of the target is stretched and bended forward, which leads to a bulge formation and to a damage of the elements on its top. The damage of the elements at time 550  $\mu$ s Fig. 5(d), inside the plate, results from a shearing process caused by different stress states between elements which are under tension (on the bottom of the plate) and elements which are not severely deformed (outside the zone of the direct projectile path). This stage includes a combination of shear and tensile stresses beneath the projectile. In Fig. 6, the maps of shear stress, Fig. 6(a), and equivalent stress, Fig. 6(b) and thermal effects, Fig. 6(c), are presented. According to the numerical calculations, the deformation induces a temperature rise on the projectile periphery which has not exceeded 600°C. Directly beneath the projectile nose, a

temperature increase reaches almost its melting range. No appreciable adiabatic overheating is found by the simulation.

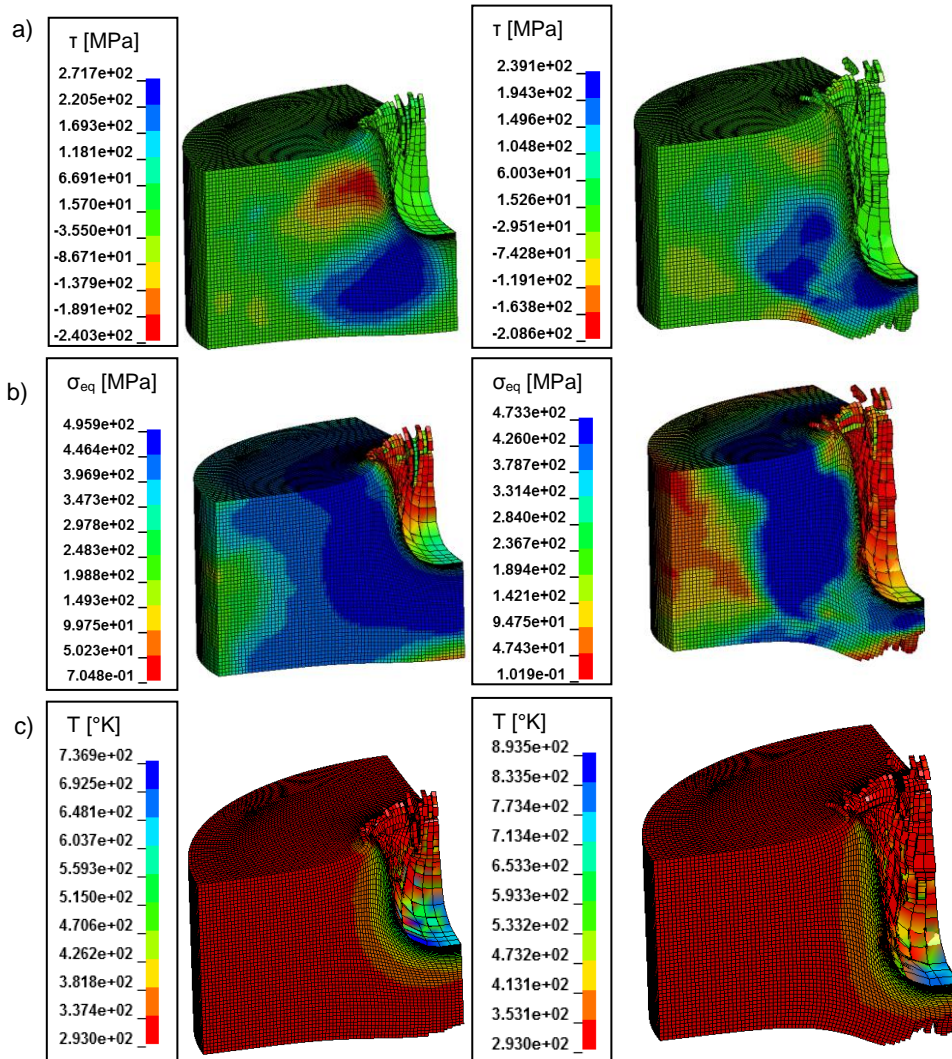


Fig.6: Maps of: (a) shear stresses, (b) equivalent stresses and (c) temperature at 140  $\mu\text{s}$  and 530  $\mu\text{s}$ .

The discing failure mode occurred in AA7020-T651 seems to be described correctly by the discussed numerical model. However, the material failure caused by for the lower impact velocity (i.e. plugging) could not be modeled properly with the chosen set of the material parameters, Table 1. The numerical results of the impact with an initial projectile velocity  $v_0=1100$  m/s are presented in Fig. 7(a). The figure shows that a plug is separated from the material, however its shape does not correspond to the shape observed in the experiment. No bulge has been created, either. To obtain the plugging failure mode, another simulation is proposed. The applied set of the  $D_i$  parameters is slightly modified but the other task conditions are identical to those discussed previously. The  $D_4$  -  $D_5$  parameters of the fracture strain, Eq. (2), are taken from [18] in which the properties of an alloy AA5083-H116 are described. By using the fracture model, in which the  $D_4$  and  $D_5$  are equal to 0.15 and 16.8, it is possible to obtain a plug of a shape and mass close to the experimental one, Figs. 7(b) – (d). Conversely, the model, due to which the plugging is calculated properly, cannot predict the discing failure for higher impact velocities. This observation will be subjected to more detailed investigation.

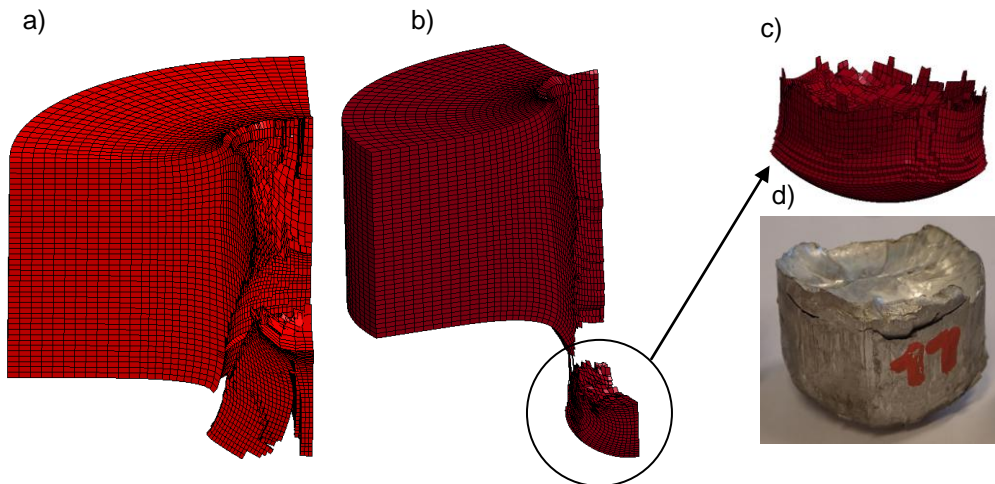


Fig.7: Modeling of a plugging failure mode at impact velocity 1100 m/s resulted from simulations in which (a)  $D_4 = 0.016$  and  $D_5 = 0.15$  (b)  $D_4 = 0.15$  and  $D_5 = 16.8$  (c) magnification of a plug obtained numerically and (d) experimental plug.

In Fig. 8, the numerical and experimental curves presenting the dependence between initial and residual velocity are shown. The ballistic limit curve is obtained using the material and fracture model defined by the parameters from Table 1.

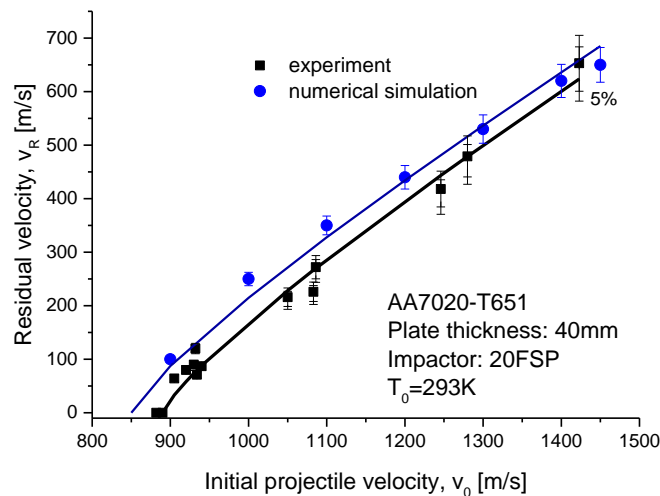


Fig.8: Numerically predicted ballistic curve and comparison with experimental data for 40 mm thick AA7020-T651 plates impacted by 20 mm FSPs.

The calculated ballistic limit is close to 840 m/s which is 10% lower compared to the experimental result, i.e.  $v_{bl,exp} \approx 890$  m/s. Due to an inaccurate value of the ballistic limit velocity, the experimental and numerical data do not coincide - the ballistic limit curve obtained numerically overestimates values of the residual velocity.

## 5 Summary

The ballistic impact test has been performed by using non-axisymmetric projectiles, 20 mm FSPs, against 40 mm thick aluminum plates in an impact velocity range from 850 m/s to 1500 m/s. The ballistic limit velocity for the discussed configuration is close to 900 m/s. In the case of the impact



velocities lower than 1200 m/s, the targets fail due to the shear plugging. With increasing impact velocity, a discing failure is observed.

The numerical simulation of the ballistic tests using LS-DYNA is treated as a tool due to which it is possible to understand the phenomena which are observed in the target plates. Classical Lagrangian finite elements with the implemented Johnson – Cook constitutive and fracture models are used, Eqs. (1) – (3). The parameters of the model and the strain at fracture were obtained experimentally (without  $D_4 - D_5$ ). It can be concluded that the numerically obtained target response is in good agreement with the experimental observations. Both observed failure modes of the target plates have been properly described by the computational model but this has been achieved by an application of different values of the parameters  $D_4$  and  $D_5$  of the fracture strain

## 6 Literature

- [1] [www.aubertduval.com](http://www.aubertduval.com)
- [2] Harpell GA, Kavesh S, Palley I, Prevorsek DC. Ballistic-resistant article. U.S. Patent No. 4.403.012 1983.
- [3] MIL-P-46593A (NOTICE 1), MILITARY SPECIFICATION: PROJECTILE, CALIBERS .22, .30, .50, AND 20MM FRAGMENT-SIMULATING (01-JUN-1996) [S/S BY MIL-DTL-46593B].
- [4] Procedures for evaluating the protection level of logistic and light armored vehicles, Vol. 1 AEP - 55, 2005.
- [5] Johnson GR, Cook WH. A constitutive model and data for metals subjected to large strains, high strain rates and high temperatures. 7th Intal Symp on Ballistics 1983.
- [6] Johnson GR, Cook WH. Fracture characteristics of three metals subjected to various strains, strain rates, temperatures and pressures. Eng Fract Mech 1985;21.1:31–48.
- [7] [www.lstc.com/pdf/ls-dyna\\_971\\_manual\\_k.pdf](http://www.lstc.com/pdf/ls-dyna_971_manual_k.pdf)
- [8] Kerisit et al.: Ballistic performance of Al-based nanocomposites developed by the powder metallurgy route against rods & fragments, 28th Int Symp on Ballistics, Atlanta 2014
- [9] Zukas J. Impact dynamics. 1th ed. New York: John Wiley & Sons, 1982.
- [10] Woodward RL. The interrelation of failure modes observed in the penetration of metallic targets. Int J Impact Eng 1984;2.2:121-9.
- [11]. Børvik T, Langseth M, Hopperstad OS, Malo KA. Perforation of 12mm thick steel plates by 20mm diameter projectiles with flat, hemispherical and conical noses: part I: experimental study. Int J Impact Eng 2002;27.1: 19-35.
- [12]. Børvik T, Langseth M, Hopperstad OS, Malo KA. Perforation of 12mm thick steel plates by 20mm diameter projectiles with flat, hemispherical and conical noses: part II: numerical simulations. Int J Impact Eng 2002;27.1: 37-64.
- [13] Brar NS, Joshi VS, Harris BW. Constitutive model constants for Al7075-T651 and Al7075-T6. AIP Conf Proc 2009;1195.1:945-8.
- [14] Børvik T, Hopperstad OS, Berstad T, Langseth M. A computational model of viscoplasticity and ductile damage for impact and penetration. Eur J Mech A/Solids 2001;20:685-712.
- [15] Børvik T, Langseth M, Hopperstad OS, Malo KA. Ballistic penetration of steel plates. Int J Impact Eng 1999;22.9: 855-86.
- [16] Børvik T, Hopperstad OS, Pedersen KO. Quasi-brittle fracture during structural impact of AA7075-T651 aluminium plates. Int J Impact Eng 2010;37.5:537-51.
- [17] Schwer LE, Windsor CA. Aluminum Plate Perforation: A Comparative Case Study Using Lagrange With Erosion, Multi-Material ALE, and Smooth Particle Hydrodynamics. 7th European LS-DYNA conference 2009.
- [18] Clausen AH, Børvik T, Hopperstad OS, Benallal A. Flow and fracture characteristics of aluminium alloy AA5083–H116 as function of strain rate, temperature and triaxiality. Mat Sci Eng A 2004;364.1:260-72.